Dalton Transactions

Accepted Manuscript

ROYAL SOCIETY OF CHEMISTRY

www.rsc.org/dalton

Dalton Transactions

RSCPublishing

ARTICLE

High-effective photocatalytic properties and interfacial transfer efficiencies of charge carriers for the novel Ag_2CO_3/AgX heterojunctions achieved by surface modification

Cite this: DOI: 10.1039/xoxxoooooox

Received ooth January 2014,
Accepted ooth January 2014

DOI: 10.1039/xoxxoooooox

www.rsc.org/

Hongjun Dong,[ab] Gang Chen,*[a] Jingxue Sun,[a] Yujie Feng*[c], Chunmei Li,[a] Guihong Xiong[a] and Chade Lv[a]

The novel Ag_2CO_3/AgX heterojunctions are achieved from the surface modification of Ag_2CO_3 with AgX (X = Cl, Br and I) nanoparticles by a facilely efficient ion-exchange method, which distinctly enhance degradation activity for typical RhB, MB, and MO dyes compared with Ag_2CO_3. The formation of heterostructure is evidenced by XRD, SEM, EDS, XPS and UV-vis DRS analyses, which indicates the bonding interaction between Ag_2CO_3 and AgX reduces the transfer potential barrier of charge carriers on their interface and extends visible light harvest at 480-640 nm. Photocurrent responses and PL spectra demonstrate Ag_2CO_3/AgX heterojunctions can effectively separate electron-hole pairs and suppress their recombination. The dye sensitization effect indicates that the effective electronic injection from RhB to heterojunction is in favor of improving photocatalytic ability. The possible transferred and separated behaviors of electron-hole pairs and photocatalytic mechanisms are illustrated in detail.

Introduction

During the past decades, photocatalysis as a "green" technique has been extensively researched in the field of wastewater treatment because most kinds of pollutants can be degraded completely by semiconductor photocatalysts under the visible light.[1] The plenty of efforts have been made to explore high-efficiency photocatalysts for the decomposition of organic contaminants.[2] However, to search new photocatalysts with high catalytic activity and research the transfer and separation behaviors of charge carriers[3] still possess a big challenge so far.

It is well known that the generation of electron-hole pairs upon light irradiation promotes the formation of powerful oxidative activated species on the photocatalyst surface to decompose organic pollutants.[4] The most photocatalysts, owing to so fast recombination rate of electron-hole pairs on the surface, are restricted in industrial applications.[3a] Therefore, inhibiting the recombination of internal charge carriers is essential for improving the net charge transfer and separation efficiency of photocatalyst.[5] For this purpose, the variously effective strategies have been successfully explored and developed, such as controlling doped-defect,[6] loading noble metal[7] and constructing heterostructure etc.[8] In consequence, tailoring photocatalyst properties by fabricating designed structure is indispensable to improving transfer and separation efficiency of charge carriers. It has demonstrated that hybridized two semiconductors, bringing about construction of heterostructure, can greatly decrease recombination probability of electron-hole pairs and increase lifetime.[9] For instance, TiO_2/ITO/SWCNTs[10] and Cu_2O/TiO_2[11] show the improved photoelectrochemical activity as well as g-C_3N_4/$BiPO_4$[12] and SnO_2/TiO_2[13] also exhibit the enhanced photocatalytic ability, which ascribes to the efficient transfer and separation of charge carriers in heterojunctions.

It is the heterostructure that dominates some behaviors of charge carriers, such as the transportation direction, separation distance and recombination rate and so on.[14] Therefore, rational designing heterojunction with rapid transfer and separation efficiency and studying effect of heterostructure on the behavior of charge carriers are important and desired for the exploitation of high-effective photocatalysts. Although there have been some reports about discussion for the transfer behavior of charge carriers in heterojunctions,[15] the better comprehending the transfer, separation, and recombination process of electron-hole pairs still possesses an important significance to probe into the intrinsic reasons of the enhanced photocatalytic activity. As a target, we design and synthesize heterojunctions using a simple method and further investigate their transferred and separated behavior of charge carriers.

The reported Ag_3PO_4[16] and Ag_2CO_3[17] photocatalysts have high-efficiency degradation ability for multifarious dyes, but they easily take place photocorrosion under visible irradiation.[18] However, when the silver phosphate surface is modified with silver halide to construct AgX/Ag_3PO_4 heterojunction, it not only improves photocatalytic ability but also increases the stability of samples.[19] Meanwhile, the various photocatalysts modified by silver halide also

attract attentions of the most researchers. Such as Ag/AgX/BiOX,[20] AgBr/$BiPO_4$,[21] Ag_3VO_4/AgBr/Ag,[22] Ag/AgX-CNTs,[23] Ag/AgBr/g-C_3N_4,[24] Ag/AgBr/TiO_2/RGO[25] and so forth all exhibit improved photocatalytic ability.

To our knowledge, no researches on the composite Ag_2CO_3/AgX photocatalysts have been reported. In this work, the unique Ag_2CO_3/AgX heterojunctions achieved by modifying silver carbonate surface with silver halide nanoparticles are prepared with a facilely efficient ion-exchange method. These heterojunctions exhibit distinctly enhanced degradation ability for the typical RhB, MB and MO dyes. The possible transferred and separated behaviors of charge carriers and photocatalytic mechanisms are discussed in depth.

Experimental

Preparation and Characterization. The Ag_2CO_3 samples were prepared by our previous reported method.[17] The Ag_2CO_3/AgX heterojunctions were prepared by ion-exchange method. As-prepared Ag_2CO_3 samples (1g) were put into the beaker with 30 ml H_2O. After ultrasonic dispersion 30 min, suspensions were quickly added to the KX (X = Cl, Br and I) solutions (30 ml, 10 mmol L^{-1}), and then aged 4 h. The precipitations were washed in turn with secondary distilled water and absolute ethanol to dissolve any unreacted raw materials. Lastly, the Ag_2CO_3/AgX heterostructure products were blow-dried using blower under atmosphere at room temperature.

The phases of the Ag_2CO_3 and Ag_2CO_3/AgX samples were characterized by powder X-ray diffractometer (XRD, Rigaku D/max-2000) equipped with a Cu-Kα radiation at a scanning rate of 5° min^{-1} in the 2θ range of 10 - 90°. X-ray tube voltage and current were set at 45 kV and 50 mA, respectively. The morphologies of the samples were characterized by field-emission scanning electron microscopy (FESEM, FEI QUANTA 200F). X-ray photoelectron spectroscopy (XPS) analysis was measured on an American electronics physical HI5700ESCA system with X-ray photoelectron spectroscope using Al Kα (1486.6 eV) monochromatic X-ray radiation. The peak positions were corrected against the C 1s peak (284.6 eV). The ultraviolet-visible diffuse reflectance spectra (UV-vis DRS) of the samples were recorded on a UV-vis spectrophotometer (PG, TU-1901) at room temperature with $BaSO_4$ as the background between 200 and 900 nm. The photoluminescence (PL) spectra were measured with a Perkin Elmer LS55 at room temperature. The nitrogen adsorption and desorption isotherm and Brunauer-Emmett-Teller (BET) specific surface area were measured at 77K using an AUTOSORB-1 Surface Area and Pore Size Analyzer.

Photocatalytic and Photoelectrochemical Measurements. The degradations of the organic dyes were carried out with 0.03 g of the Ag_2CO_3 and Ag_2CO_3/AgX powders suspended in the methyl orange (MO), rhodamine B (RhB) or methylene blue (MB) solutions (10 mg L^{-1}, 100 ml). Then the degradation reaction system was irradiated with a 300 W Xe arc lamp (Trusttech PLS-SXE 300, Beijing) equipped with an ultraviolet cutoff filter or band pass filter to provide visible light with $\lambda \geq$ 400nm or monochromatic wavelength with 550 nm and 420 nm ($\Delta\lambda$ = ± 15nm), respectively. Before the suspensions were irradiated, they were carried out about 2 min of ultrasonic process and magnetically stirred for 50 min in the dark to complete the adsorption-desorption equilibrium between dyes and photocatalysts. Lastly, the above suspensions were exposed to the visible light irradiation under magnetic stirring. UV-vis spectrophotometer (PG, TU-1901) monitored the absorbance of dye solutions at intervals of 5 min in degradation process. Before measurement, the photocatalyst was removed from the photocatalytic reaction system by centrifugalization.

The photoelectrochemical characteristics were measured in a CHI604C electrochemical working station using a standard three-compartment cell under Xe arc lamp irradiation with 300 W. The Ag_2CO_3 or Ag_2CO_3/AgX composites coated FTO glass, a piece of Pt sheet, a Ag/AgCl electrode and 0.01 M sodium carbonate were used as the working electrode, the counter-electrode, the reference electrode and the electrolyte, respectively.

Results and discussion

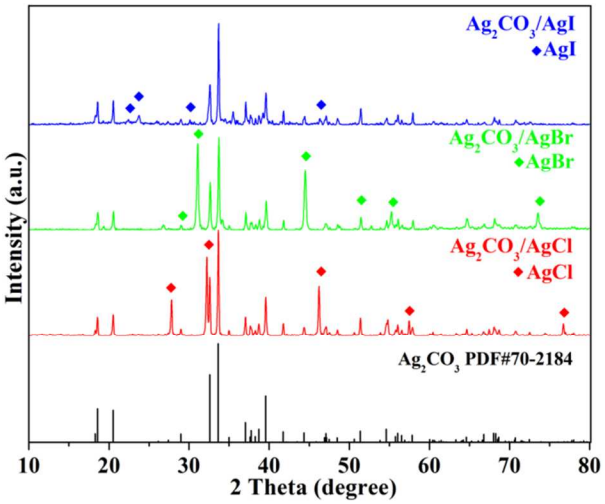

Fig. 1 XRD patterns of Ag_2CO_3/AgX samples.

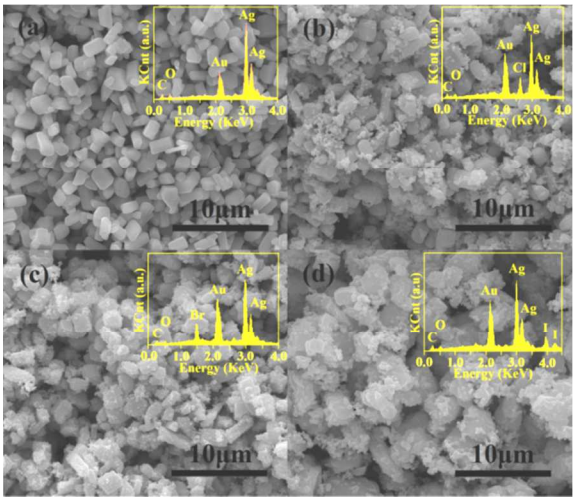

Fig. 2 FESEM images and EDS spectra (insert) of Ag_2CO_3 (a) and Ag_2CO_3/AgX (Cl (b), Br(c) and I (d)) samples.

The characteristic peaks appearing at each XRD pattern in Fig. 1 are well indexed to Ag_2CO_3 and AgX (X = Cl, Br and I), which demonstrates the as-prepared samples are composed of Ag_2CO_3 and AgX, respectively. The metal Ag or other

characteristic peaks are not detected. All the sharp and intense diffraction peaks reveal the samples have the high crystallinity. According to FESEM image in Fig. 2(a), Ag_2CO_3 sample displays smooth surface. By comparison, as shown the FESEM images in Fig. 2(b-d), the appearances of Ag_2CO_3/AgX samples change into obviously rough morphologies owing to the Ag_2CO_3 surface covered by abundant AgX nanoparticles, which is evidenced by the high-magnification FESEM images of Ag_2CO_3/AgX samples (see Fig. S1 in the ESI†). In addition, the EDS spectra of all the samples (the insert of Fig. 2(a-d) display the Ag_2CO_3/AgX samples contain Cl, Br and I elements, respectively. All above results indicate that the Ag_2CO_3/AgX heterojunctions are constructed via the surface modification of Ag_2CO_3 with AgX nanoparticles.

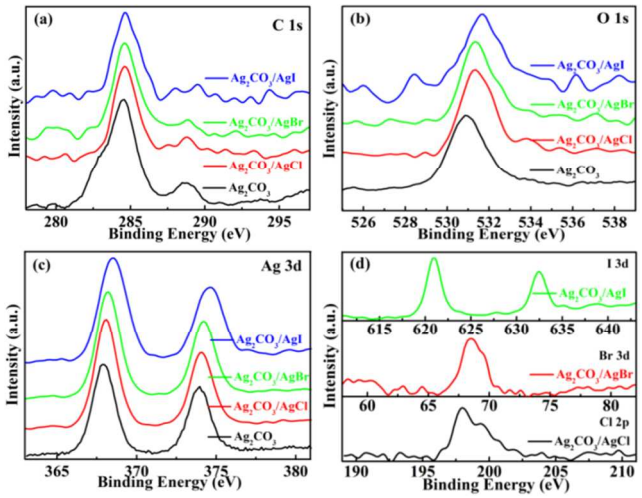

Fig. 3 High-resolution XPS spectra of Ag_2CO_3 and Ag_2CO_3/AgX samples.

XPS spectra are employed to gain a better insight into the surface state and interaction characteristics between Ag_2CO_3 and AgX nanoparticles in heterojunctions. The total XPS spectra of Ag_2CO_3/AgX heterojunctions (see Fig. S2 in the ESI†) display the different binding energy peaks are assigned to Ag 3d, Ag 3p, O 1s, C 1s, Cl 2p (a), Br 3d (b) and I 3d (c) states, and to Ag and O auger features, respectively. From the high-resolution XPS spectra of Ag_2CO_3 and Ag_2CO_3/AgX heterojunctions in Fig. 3, the wide and asymmetric shapes of C 1s and O 1s spectra indicate they have different chemical states.[26] The peaks at 284.6 eV and 288-289 eV in Fig. 3(a) are due to C element in Ag_2CO_3 and hydrocarbon contaminants, respectively;[27] The peak at 530.6 eV and shoulder peak at the high binding energy in Fig. 3(b) belong to O 1s state of Ag_2CO_3 and adsorbed hydroxyl species, respectively.[28] Moreover, the XPS spectra of Ag 3d in Fig. 3(c) are attribute to the Ag $3d_{5/2}$ and $3d_{3/2}$ states at 367.9 eV and 374.0 eV, respectively. Contrary to C 1s and O 1s, the shape of no-broadening and symmetric peaks for Ag 3d XPS spectra indicates that Ag may only possess one chemical state. In other words, no metal Ag generates on the Ag_2CO_3/AgX heterojunctions surface. Fig. 3(d) exhibits the obvious emission peaks deriving from $2p_3$ and $2p_1$ of Cl (197.9 and 199.5 eV), $3d_{5/2}$ and $3d_{3/2}$ of Br (68.4 and 69.7 eV) as well as $3d_5$ and $3d_3$ of I (621.0 and 632.5 eV), respectively, which is consistent with the results of EDS spectra. It is noticed that the peaks of O in Ag_2CO_3/AgX (X = Cl, Br and I) relative to Ag_2CO_3 shift 0.6, 0.8 and 1.1 eV toward the high binding energy, respectively, which demonstrates bonding effects between Ag^+ and CO_3^{2-} on the Ag_2CO_3 surface are enhanced. This shift phenomenon may result from connection between Ag_2CO_3 and AgX by bonding interaction on their interface, because the shift of binding energy likely arises from bonding interaction and electron transfer among semiconductors.[29] Similarly, the peaks of Ag $3d_{5/2}$ in Ag_2CO_3/AgX (X = Cl, Br and I) also shift 0.2, 0.3 and 0.7 eV to the high binding energy, respectively, which further indicates bonding interaction on the interface between Ag_2CO_3 and AgX.

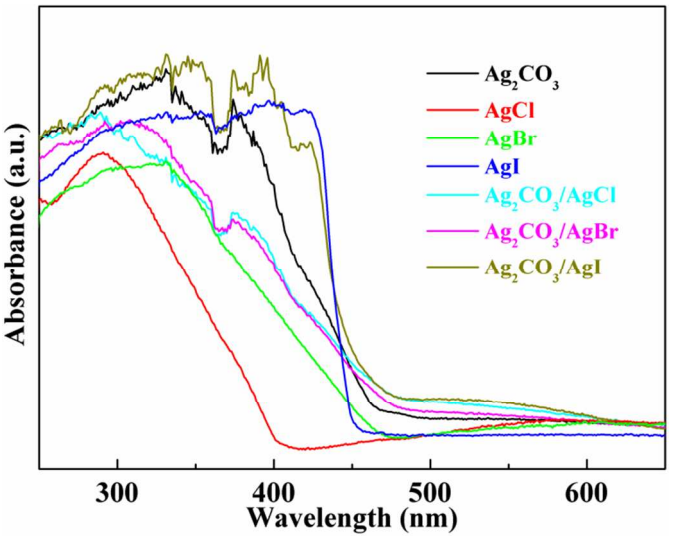

Fig. 4 UV-vis DRS spectra of Ag_2CO_3, AgX and Ag_2CO_3/AgX samples.

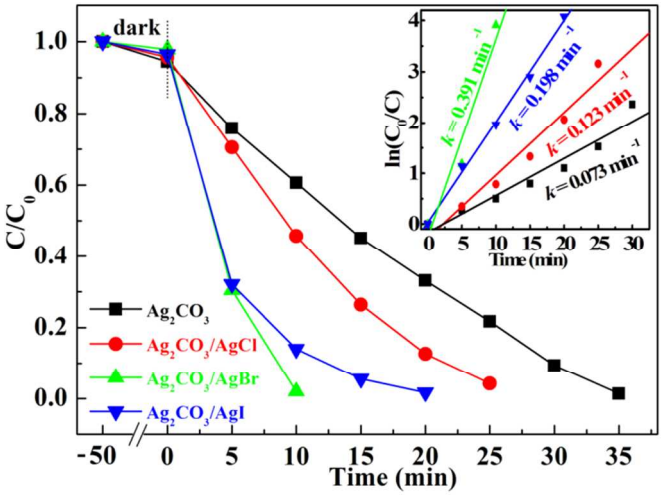

Fig. 5 Dynamic curves and plots of $\ln(c_0/c)$ versus time (insert) of RhB solutions over Ag_2CO_3 and Ag_2CO_3/AgX samples.

The light harvest and heterostructure information are connected with the absorption variation before and after formation of the heterojunction. The UV-vis DRS spectra of Ag_2CO_3, AgX and Ag_2CO_3/AgX samples in Fig. 4 indicate that

all samples except for AgCl exhibit strong visible light absorption. The changes of absorption edge of may result from optical characteristics of AgX themselves on the Ag_2CO_3 surface. More remarkably, compared with Ag_2CO_3 and AgX, absorption intensities of Ag_2CO_3/AgX heterojunctions are all interesting enhancement at 480-640 nm. Some reports believe that this absorption region may arise from Ag surface plasmon resonance effect,[21-25] but it is eliminated at present experiments because of no Ag generation on the sample surface evidenced in XRD and XPS analyses. Furthermore, the bonding interaction can effectively decrease contact barrier and strengthen electronic coupling of tow semiconductors, thus resulting in the improved absorption of heterojunctions at long wavelength.[29b] Therefore, the absorption at 480-640 nm may be due to the electronic coupling effect on the interface between Ag_2CO_3 and AgX nanoparticles.

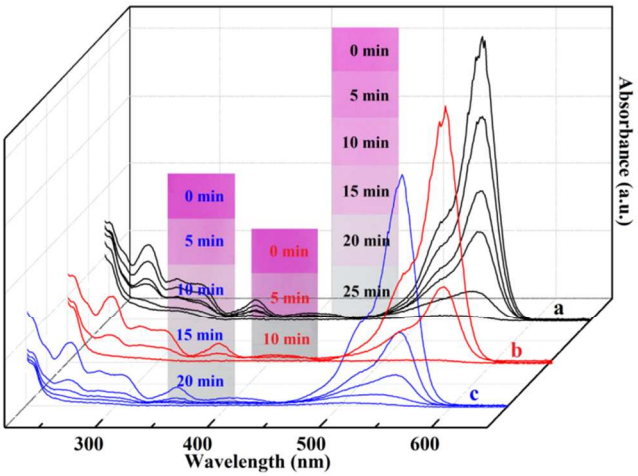

Fig. 6 Absorbance and color variations of RhB solutions over Ag_2CO_3/AgX (X = Cl (a), Br (b) and I (c)) samples.

The photocatalytic activity of samples is evaluated by degradation of RhB solution. When KX solutions are added to 30 ml, Ag_2CO_3/AgX samples exhibit the higher degradation activity (see Fig. S3 in the ESI†). Fig. 5 shows the contrast of dynamic curves for RhB degradation over Ag_2CO_3 and Ag_2CO_3/AgX heterojunctions. After the Ag_2CO_3 surface are modified by AgX nanoparticles, Ag_2CO_3/AgX (X = Cl, Br and I) heterojunctions completely decompose RhB within 25, 10 and 20 min, respectively, which are lower than that of Ag_2CO_3 (35 min). Moreover, the kinetic curves of RhB degradation can be approximated as a pseudo-first-order process.[30] The plots of $\ln(c_0/c)$ versus time of RhB solutions are shown in the insert of Fig. 5. By use of fitting results for these plots, we achieve that the removal rate constants k of RhB over Ag_2CO_3/AgX (X = Cl, Br and I) are 0.123, 0.391 and 0.198 min^{-1}, which amazingly reach about 1.68, 5.36 and 2.71 times as much as that over Ag_2CO_3 (0.073 min^{-1}), respectively. Furthermore, the absorbance and color variations of RhB solutions in the photocatalytic reaction are performed (Fig. 6). No-shifting of the maximum absorption peaks of RhB solutions at 554 nm and the vanishing absorptions of ultraviolet region at 250-380 nm prove that the benzene/heterocyclic rings of RhB molecule may be destroyed, leading to the thorough decomposition of RhB.[17] Meanwhile, the degradation activities of Ag_2CO_3/AgX heterojunctions are also higher than that of pure AgX sample (see Fig. S4 in the ESI†). In addition, the cycle experiments are carried out because stability of photocatalysts is important in practical application (see Fig. S5 in the ESI†). The results show that degradation ability of Ag_2CO_3 for RhB dye presents obvious reduction after two circles. In contrast, after modification with AgX nanoparticles, cycle runs of Ag_2CO_3/AgX heterojunctions reach up to four times. Therefore, Ag_2CO_3/AgX heterojunctions exert the better degradation activity and higher stability than Ag_2CO_3. Considering the specific surface area has an important effect on photocatalytic ability, N_2 adsorption and desorption isotherm and the BET specific surface area of all samples are measured (see Fig. S6 in the ESI†). The specific surface area of 1.739, 2.055 and 1.816 $m^2\ g^{-1}$ for Ag_2CO_3/AgX (X = Cl, Br and I) samples are almost twice that of Ag_2CO_3 (0.914 $m^2\ g^{-1}$),[28] which may be due to the abundant AgX nanoparticles on the Ag_2CO_3 surface. It suggests that the specific surface area has an effect on the improved degradation activity of Ag_2CO_3/AgX heterojunctions.

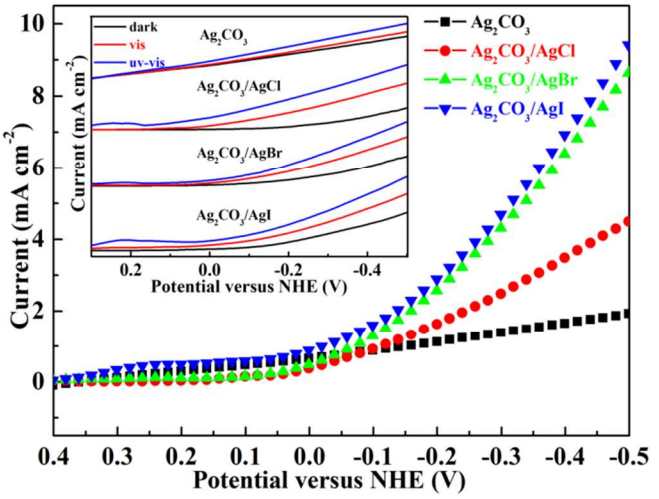

Fig. 7 Photocurrent responses of Ag_2CO_3 and Ag_2CO_3/AgX photoelectrodes under visible light with $\lambda \geq 400$ nm and different illumination conditions (insert).

The magnitude of the photocurrent represents the charge collection efficiency of the electrode surface, and indirectly indicates the separated efficiency of electron-hole pairs.[31] From the insert of Fig. 7, all photoelectrodes are prompt in generating photocurrent under visible and UV-visible light. Ag_2CO_3/AgX photoelectrodes yield the greater photocurrent than Ag_2CO_3 photoelectrode under visible light in Fig. 7. In order to explore the improved photocurrent, the relative band positions of Ag_2CO_3 and AgX (X = Cl, Br and I) are calculated (see Table S1 in the ESI†). The external electric field and the effectively interfacial bonding interaction between Ag_2CO_3 and AgX may result in the lower contact barrier, which is in favor of the transfer of charge carriers. In Ag_2CO_3/AgCl heterojunction, the transfer of charge carriers on the interface is thermodynamicly

promoted owing to the suitable band position of Ag_2CO_3 (E_{CB} = 0.29 eV and E_{VB} = 2.75 eV) and AgCl (E_{CB} = 0.06 eV and E_{VB} = 3.31 eV). Electrons and holes can migrate from the CB and VB of AgCl to that of Ag_2CO_3 under external electric field, respectively. The result leads to increasing charge carrier concentrations in CB and VB of Ag_2CO_3, which improves photocurrent intensity. However, because the broad band gap with 3.25 eV of AgCl cannot absorb visible light, no redundant photogenerated charge carriers are produced. The lower carrier concentrations of AgCl at the room temperature only bring about the less extent enhancement of photocurrent. Furthermore, when the Ag_2CO_3 surface is modified by AgBr(AgI) nanoparticles, because of better matching energy band position (AgBr: E_{CB} = 0.04 eV and E_{VB} = 2.64 eV, AgI: E_{CB} = -0.42 eV and E_{VB} = 2.38 eV,), the electrons and holes migrate from the CB of AgBr(AgI) and VB of Ag_2CO_3 to the CB of Ag_2CO_3 and VB of AgBr(AgI), respectively. It increases the amount of net charge carriers and improves their separated efficiency. In addition, the narrow band gap of AgBr with 2.6 eV and AgI with 2.8 eV can harvest visible light to produce the much photogenerated charge carriers. Thus, the more intense photocurrent responses are produced in Ag_2CO_3/AgBr(AgI) heterojunctions.

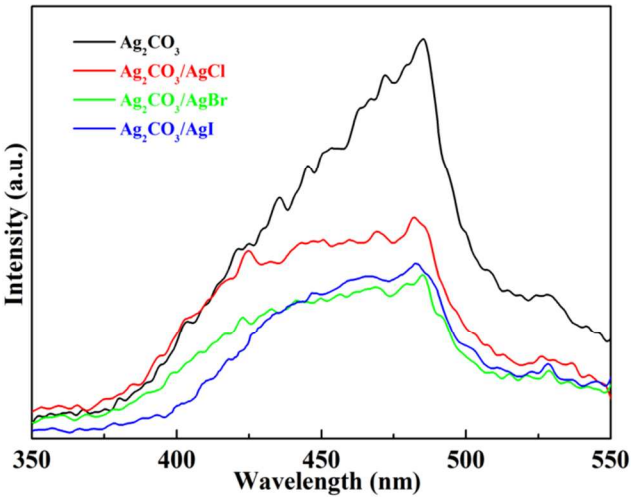

Fig. 8 PL spectra of Ag_2CO_3 and AgX/Ag_2CO_3 samples (λ_{ex} = 350 nm).

Furthermore, the photoluminescent (PL) spectra can be regarded as an effective approach to comprehend the separated capacity of charge carriers.[32] The obvious fluorescence quenching takes place in the PL spectra of Ag_2CO_3/AgX heterojunctions compared with that of Ag_2CO_3 in Fig. 8. Unlike photocurrent responses, the holes of AgCl cannot transfer to the VB of Ag_2CO_3 after attaining equilibrium at the interface because of no external electric field. In addition, AgCl is not excited under the exceeding 315 nm (3.25 eV). Consequently, the light absorption efficiency of Ag_2CO_3 decreases owing to the shield effect resulting from surface AgCl nanoparticles, which may be responsible for PL reduction of Ag_2CO_3/AgCl heterojunctions. By contrast, the quenching extent of Ag_2CO_3/AgBr(AgI) heterojunctions exhibits more conspicuous than Ag_2CO_3/AgCl, which may ascribe the interfacial transfer of charge carriers between Ag_2CO_3 and AgBr(AgI). Using excitation wavelength of 350 nm (2.93 eV), AgBr and AgI are also excited besides Ag_2CO_3. Thus electrons transfer from CB of AgBr(AgI) to that of Ag_2CO_3 as well as holes transfer from VB of Ag_2CO_3 to that of AgBr(AgI), giving rise to the recombination rate decrease thus resulting in the more obvious PL quenching. We deduce that one important reason of the enhanced photocatalytic ability for the Ag_2CO_3/AgX heterojunctions may originate from the increase of net charge carrier quantities and improvement of their transferred and separated efficiency.

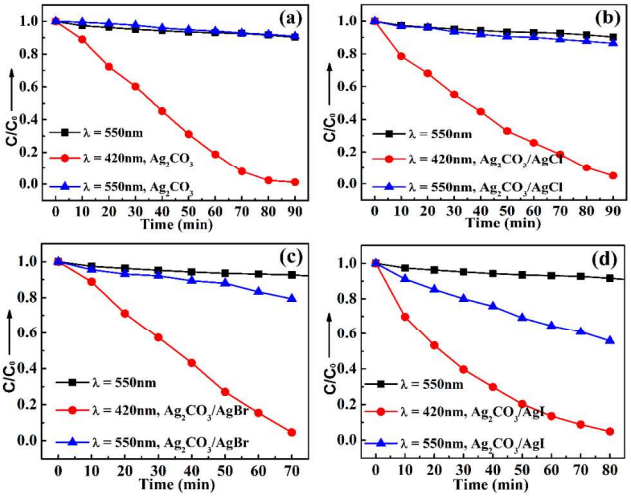

Fig. 9 Dynamic curves of RhB solutions over Ag_2CO_3 and AgX/Ag_2CO_3 under the different monochromatic wavelength

The silver halide exhibits dye sensitization effect to some extent,[33] which is usually little considered at previously photocatalytic researches.[34] Therefore, the interaction of dyes and Ag_2CO_3/AgX heterojunctions should be indispensably taken into account to investigate charge carrier transfer process. The monochromatic wavelength irradiation method is usually applied to identify existence of dye sensitization effect[26] according to the different absorption regions of RhB (500-580 nm) and catalysts (< 500 nm). As shown in Fig. 9(a), performing monochromatic wavelength with 420 nm to excite the Ag_2CO_3 sample, the degradation efficiency of RhB reaches approximately 100% after 90 min. In contrast, when monochromatic wavelength with 550 nm is used to excite RhB molecules, the result exhibits that the approximate 5% of RhB is degraded within 90 min, which is the same as decomposition extent without any photocatalysts. No occurring dye sensitization effect demonstrates the transfer of electrons between RhB and Ag_2CO_3 is insignificant and neglectful. However, in Fig. 9 (b-d), upon exciting Ag_2CO_3/AgX (X = Cl, Br and I) heterojunctions by monochromatic wavelength with 420 nm, approximate 100% of RhB molecules are decomposed within 90, 70 and 80 min, respectively. In comparison, the distinct removal rates of 10%, 20% and 40% for RhB are still

achieved, even only exciting RhB molecules employing monochromatic wavelength with 550 nm. It indicates that the dye sensitization effects occur in surface AgX nanoparticles because of eliminating interaction between RhB and Ag_2CO_3. The energy level of the lowest unoccupied molecular orbital (LUMO) and the highest occupied molecular orbital (HOMO) of RhB are -1.0 eV and 1.1 eV,[35] respectively. AgX can act as an effective electron acceptor due to their lower CB potential. The photoexcited electrons in LUMO of RhB will preferentially transfer to the CB of AgX, leading to the increased aggregation of electron quantities, and then immediately migrate to the CB of Ag_2CO_3 to generate the abundant activated species participating in photocatalytic reaction. Therefore, the other reason of the photocatalytic enhancement for RhB degradation may be attributed to the dye sensitization effect.

It is noticed that the dye sensitization effect displays more and more intense in sequence from Ag_2CO_3/AgCl, Ag_2CO_3/AgBr to Ag_2CO_3/AgI. The potential energy difference between the CB of AgX and the LUMO of RhB provides thermodynamic requirement for dye sensitization effect occurring but cannot determine the sensitized extent. At present experimental results, the dye sensitization effect may be controlled by the transferred and separated efficiency of charge carriers for Ag_2CO_3/AgX heterojunctions. The lower VB position of AgCl cannot accept photogenerated holes from Ag_2CO_3 in Ag_2CO_3/AgCl heterojunction, and its suitable CB position may merely serve as a medium of electron transfer from RhB to Ag_2CO_3. The lower electronic transfer efficiency results in low-level dye sensitization effect. In contrast, the CB and VB of AgBr can serve as electrons donor and holes acceptor, respectively, owing to their matching position with Ag_2CO_3, which enhances the transferred and separated efficiency of charge carriers. Therefore, this can induce the rapidly electronic transfer from RhB to the CB of AgBr, leading to the more obvious dye sensitization effect. Moreover, besides the matching band position in Ag_2CO_3/AgI heterojunction, the higher CB and VB position of AgI than AgBr relative to Ag_2CO_3 may be in favor of accelerating electronic transfer and separation, which further improves the extent of dye sensitization effect.

Based on above analysis results, Fig. 10 exhibits the schematic transfer and separation behaviors of charge carriers and photocatalytic mechanisms of RhB over Ag_2CO_3/AgX. We have reported that $\cdot O_2^-$ radical has played an important role in RhB degradation process over Ag_2CO_3 samples.[28] In the Ag_2CO_3/AgCl heterojunction, the generation and separation of electron-hole pairs originate from Ag_2CO_3. AgCl as a medium of the electrons injecting from RhB to Ag_2CO_3 causes slight dye sensitization effect, which together with little enhanced visible light harvest result in the less improved degradation ability. Moreover, for Ag_2CO_3/AgBr(AgI) heterojunctions, their matching band position with Ag_2CO_3 not only facilitates the transferred and separated efficiency of charge carriers but also induces the high-extent dye sensitization effect, giving rise to the more enhanced degradation activity.

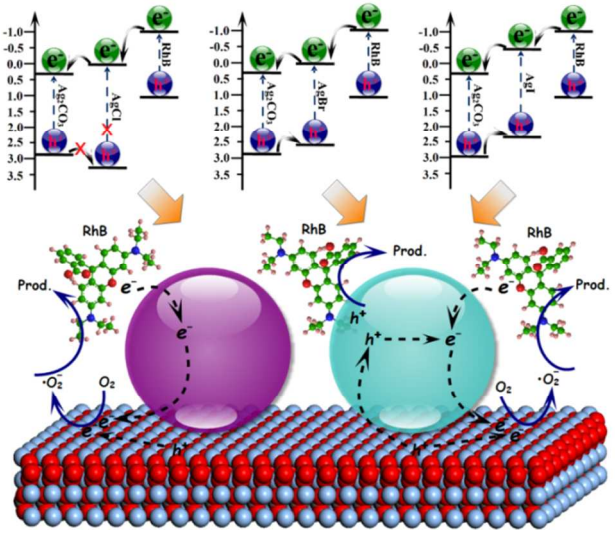

Fig. 10 Schematic transferred and separated behaviors of charge carriers and photocatalytic mechanisms of RhB over Ag_2CO_3/AgX samples.

For purpose of further verifying improved transfer and separation efficiency of charge carriers and photocatalytic activity, the degradations of typical MB and MO dyes are also carried out. Dynamic curves and absorbency variations of MB and MO solutions under visible light are carried out, respectively (see Fig. S7-S8 in the ESI†). Ag_2CO_3/AgX (X = Cl, Br and I) heterojunctions exhibit enhanced photocatalytic ability for MB decomposition in Fig. S7(a). Consuming 25, 15 and 20 min for removal MB are distinctly reduction compared with Ag_2CO_3 (30 min). Even though the relative stable azo dye MO servers as degraded target molecule in Fig. S8(a), it is still decomposed by Ag_2CO_3/AgBr(AgI) heterojunctions within 10 min, except degradation time over Ag_2CO_3/AgCl is equal to Ag_2CO_3 (20 min). Furthermore, as shown in Fig. S7(b-d) and Fig. S8(b-d), no shifting of the maximum absorption peak and vanishing absorbance of ultraviolet region at 250-380 nm for MB and MO solutions further prove that dye molecules are degraded completely. Here the improved degradation ability further affords credible evidence for the improved transfer and separation efficiency of charge carriers owing to construction of Ag_2CO_3/AgX heterojunctions by the surface modification of Ag_2CO_3 with AgX nanoparticles.

Conclusions

In summary, the novel Ag_2CO_3/AgX heterojunctions are achieved from the surface modification of Ag_2CO_3 with AgX nanoparticles by a facilely efficient ion-exchange method, which improve the photocatalytic activity and stability for RhB, MB and MO dyes degradation compared with Ag_2CO_3. The bonding interaction between Ag_2CO_3 and AgX reduces the contact potential barrier of the interface which is in favor of transfer and separation of charge carriers. The dye sensitization effect increases accumulations of net electron quantities in heterojunctions, which results in generating the more activated

species. This work provides a simple preferred method for improving photocatalytic activity and stability of photocatalyst by surface modification of semiconductor nanoparticles.

Acknowledgements

This work was financially supported by the National Nature Science Foundation of China (21071036 and 21271055) and Province Natural Science Foundation of Heilongjiang Province (ZD201011). We acknowledge the State Key Laboratory of Urban Water Resource and Environment for the help in characterization.

Notes and references

[a] Department of Chemistry, Harbin Institute of Technology, Harbin 150001, P. R. China.
[b] Department of Chemistry, Baicheng Normal University, Baicheng 137000, P. R. China.
[c] State Key Laboratory of Urban Water Resource and Environment, Harbin Institute of Technology, Harbin 150090, P. R. China.

† Electronic Supplementary Information (ESI) available: [High-resolution FESEM images of Ag_2CO_3/AgX (Cl (a), Br(b) and I (c)) samples (Fig. S1); Total XPS spectra of Ag_2CO_3/AgX samples (Fig. S2); Circle runs of RhB dyes over Ag_2CO_3 (a) and Ag_2CO_3/AgX (Cl (b), Br(c) and I (d)) samples (Fig. S3); N_2 adsorption and desorption isotherm of Ag_2CO_3/AgX (Cl (a), Br(b) and I (c)) samples (Fig. S4); Dynamic curves and absorbance variations of MB and MO solutions degradation over Ag_2CO_3 and Ag_2CO_3/AgX under visible light (Fig. S5-S6); X, E_g, E_{CB}, and E_{VB} of AgCl, AgBr, AgI and Ag_2CO_3 samples (Table S1)]. See DOI: 10.1039/b000000x/

1 (a) M. Wu, X. Lin, Y. Wang, L. Wang, W. Guo, D. Qi, X. Peng, A. Hagfeldt, M. Grätzel and T. Ma, *J. Am. Chem. Soc.,* 2012, **134**, 3419-3428; (b) A. Kudo and Y. Miseki, *Chem. Soc. Rev.,* 2009, **38**, 253-278.

2 (a) X. J. Lang, X. D. Chen and J. C. Zhao, *Chem. Soc. Rev.,* 2014, **43**, 473-486; (b) W. Wu, R. Hao, F. Liu, X. Su and Y. Hou, *J. Mater. Chem. A*, 2013, **1**, 6888-6894; (c) F. Liu, Y. Jin, H. Liao, L. Cai, M. Tong and Y. Hou, *J. Mater. Chem. A*, 2013, **1**, 805-813; (d) Y. Liang, L. Shang, T. Bian, C. Zhou, D. Zhang, H. Yu, H. Xu, Z. Shi, T. Zhang, L. Z. Wua and C. H. Tung, *CrystEngComm*, 2012, **14**, 4431-4436; (e) Y. Zhang, B. Deng, T. Zhang, D. Gao, and A. W. Xu, *J. Phys. Chem. C*, 2010, **114**, 5073-5079.

3 (a) M. R. Hoffmann, S. T. Martin, W. Choi and D. W. Bahnemann, *Chem. Rev.,* 1995, **95**, 69-96; (b) Y. Q. Qu and X. F. Duan, *Chem. Soc. Rev.,* 2013, **42**, 2568-2580;

4 (a) S. X. Ouyang and J. H. Ye, *J. Am. Chem. Soc*., 2011, **133**, 7757-7763; (b) X. Li, X. Zhen, S. Meng, J. Xian, Y. Shao, X. Fu and D. Li, *Environ. Sci. Technol.,* 2013, **47**, 9911-9917.

5 I. Bedjat and P. V. Kamat, *J. Phys. Chem*., 1995, **99**, 9182-9188.

6 (a) X. J. Bai, L. Wang, R. L. Zong, Y. H. Lv, Y. Q. Sun and Y. F. Zhu, *Langmuir,* 2013, **29**, 3097-3105; (b) J. K. Zhou, L. Lv, J. Q. Yu, H. L. Li, P. Z. Guo, H. Sun and X. S. Zhao, *J. Phys. Chem. C,* 2008, **112**, 5316-5321.

7 (a) X. H. Li, X. C. Wang and M. Antonietti, *Chem. Sci.,* 2012, **3**, 2170-2174; (b) Y. Zhang, H. Fan, M. Li and H. Tian, *Dalton Trans.,* 2013, **42**, 13172-13178.

8 (a) T. Xie, L. Xu, C. Liu, J. Yang and M. Wang, *Dalton Trans.,* 2014, **43**, 2211-2220; (b) S. X. Yang, J. Gong and Y. L. Deng, *J. Mater. Chem.,* 2012, **22**, 13899-13902.

9 P. Tongying, V. V. Plashnitsa, N. Petchsang, F. Vietmeyer, G. J. Ferraudi, G. Krylova and M. Kuno, *J. Phys. Chem. Lett.,* 2012, **3**, 3234-3240.

10 T. T. Duong, Q. D. Nguyen, S. K. Hong, D. Kim, S. G. Yoon and T. H. Pham, *Adv. Mater.,* 2011, **23**, 5557-5562.

11 M. E. Wang, L. Sun, Z. Q. Lin, J. H. Cai, K. P. Xie and C. J. Lin, *Energy Environ. Sci.,* 2013, **6**, 1211-1220.

12 X. H. Peng, A. C. Santulli, E. Sutter and S. S. Wong, *Chem. Sci.,* 2012, **3**, 1262-1272.

13 X. Li and J. He, *ACS Appl. Mater. Interfaces*, 2013, **5**, 5282-5290.

14 X. Wei, T. F. Xie, L. L. Peng, W. Fu, J. S. Chen, Q. Gao, G. Y. Hong and D. J. Wang, *J. Phys. Chem. C,* 2011, **115**, 8637-8642.

15 (a) Y. C. Chen, Y. C. Pu and Y. J. Hsu, *J. Phys. Chem. C,* 2012, **116**, 2967-2975; (b) H. M. Fan, H. Y. Li, B. K. Liu, Y. C. Lu, T. F. Xie and D. J. Wang, *ACS Appl. Mater. Interfaces,* 2012, **4**, 4853-4857.

16 (a) Z. G. Yi, J. H. Ye, N. Kikugawa, T. Kako, S. X. Ouyang, H. Stuart-Williams, H. Yang, J. Y. Cao, W. J. Luo, Z. S. Li, Y. Liu and R. L. Withers, *Nat. Mater.,* 2010, **9**, 559-563; (b) D. J. Martin, N. Umezawa, X. Chen, J. Ye and J. Tang, *Energy Environ. Sci.,* 2013, **6**, 3380-3386; (c) Y. P. Bi, S. X. Ouyang, N. Umezawa, J. Y. Cao and J. H. Ye, *J. Am. Chem. Soc.,* 2011, **133**, 6490-6492.

17 H. J. Dong, G. Chen, J. X. Sun, C. M. Li, Y. G. Yu and D. H. Chen, *Appl. Catal. B: Environ.,* 2013, **134-135**, 46-54.

18 (a) C. W. Xu, Y. Y. Liu, B. B. Huang, H. Li, X. Y. Qin, X. Y. Zhang and Y. Dai, *Appl. Surf. Sci.,* 2011, **257,** 8732-8736; (b) W. G. Wang, B. Cheng, J. G. Yu, G. Liu and W. H. Fan, *Chem. Asian J*., 2012, **7**, 1902-1908.

19 (a) W. S. Wang, H. Du, R. X. Wang, T. Wen and A. W. Xu, *Nanoscale,* 2013, **5**, 3315-3321; (b) Z. H. Chen, W. L. Wang, Z. G. Zhang and X. M. Fang, *J. Phys. Chem. C,* 2013, **117**, 19346-19352; (c) Y. Bi, S. Ouyang, J. Cao and J. Ye, *Phys. Chem. Chem. Phys.,* 2011, **13**, 10071-10075.

20 H. F. Cheng, W. J. Wang, B. B. Huang, Z. Y. Wang, J. Zhan, X. Y. Qin, X. Y. Zhang and Y. Dai, *J. Mater. Chem. A,* 2013, **1**, 7131-7136.

21 H. Xu, Y. Xu, H. Li, J. Xia, J. Xiong, S. Yin, C. Huang and H. Wan, *Dalton Trans.,* 2012, **41**, 3387-3394.

22 Q. Zhu, W. S. Wang, L. Lin, G. Q. Gao, H. L. Guo, H. Du and A. W. Xu, *J. Phys. Chem. C,* 2013, **117**, 5894-5900.

23 H. Shi, J. Chen, G. Li, X. Nie, H. Zhao, P. K. Wong and T. An, *ACS Appl. Mater. Interfaces,* 2013, **5**, 6959-6967.

24 Y. S. Xu and W. D. Zhang, *ChemCatChem,* 2013, **5**, 2343-2351.

25 P. W. Wang, Y. X. Tang, Z. L. Dong, Z. Chen and T. T. Lim, *J. Mater. Chem. A,* 2013, **1**, 4718-4727.

26 M. T. Uddin, Y. Nicolas, C. Olivier, T. Toupance, L. Servant, M. M. Mu□ller, H. J. Kleebe, J. Ziegler and W. Jaegermann, *Inorg. Chem.,* 2012, **51**, 7764-7773.

27 J. F. Weaver and G. B. Hoflund, *Chem. Mater.,* 1994, **6**, 1693-1699.

28 J. B. Mu, C. L. Shao, Z. C. Guo, Z. Y. Zhang, M. Y. Zhang, P. Zhang, B. Chen and Y. C. Liu, *ACS Appl. Mater. Interfaces,* 2011, **3**, 590-596.

29 (a) L. Xu, E. M. P. Steinmiller and S. E. Skrabalak, *J. Phys. Chem. C,* 2012, **116**, 871-877; (b) X. T. Pian, B. Z. Lin, Y. L. Chen, J. D.

Kuang, K. Z. Zhang and L. M. Fu, *J. Phys. Chem. C,* 2011, **115**, 6531-6539.

30 I. K. Konstantinou and T. A. Albanis, *Appl. Catal. B: Environ.,* 2004, **49**, 1-14.

31 (a) Z. Pei, L. Ding, H. Lin, S. Weng, Z. Zheng, Y. Hou and P. Liu, *J. Mater. Chem. A,* 2013, **1**, 10099-10102; (b) Y. H. Ng, I. V. Lightcap, K. Goodwin, M. Matsumura and P. V. Kamat, *J. Phys. Chem. Lett.,* 2010, **1**, 2222-2227.

32 (a) Y. T. Liang, B. K. Vijayan, O. Lyandres, K. A. Gray and M. C. Hersam, *J. Phys. Chem. Lett.,* 2012, **3**, 1760-1765; (b) S. Martha, A. Nashim and K. M. Parida, *J. Mater. Chem. A,* 2013, **1**, 7816-7824.

33 (a) H. Gerischer and H. Selzle, *Electrochim. Acta,* 1973, **18**, 799-805; (b) M. T. Spitler, A. Ehret, R. Kietzmann and F. Willig, *J. Phys. Chem. B,* 1997, **101,** 2552-2557.

34 P. Wang, B. B. Huang, X. Y. Qin, X. Y. Zhang, Y. Dai, J. Y. Wei and M. H. Whangbo, *Angew. Chem. Int. Ed.,* 2008, **47**, 7931-7933.

35 Z. H. Zhang, Y. J. Yu and P. Wang, *ACS Appl. Mater. Interfaces,* 2012, **4**, 990-996.

Graphical Abstract

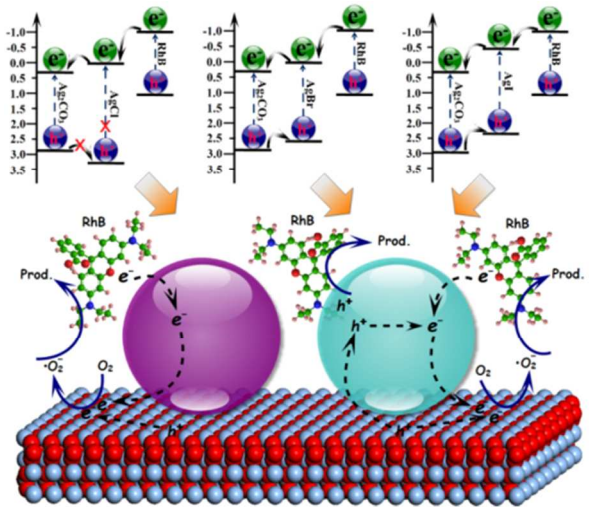

Ag_2CO_3/AgX heterojunctions are achieved from the surface modification of Ag_2CO_3 with AgX nanoparticles, which improve the photocatalytic activity and stability for dyes degradation.